PROCEEDINGS OF SCIENCE

The hadronic contribution to the running of the electromagnetic coupling and electroweak mixing angle

Teseo San José,[c,d,e,f,*] **Marco Cè,**[a] **Antoine Gérardin,**[b] **Georg von Hippel,**[e,f] **Harvey B. Meyer,**[c,d,e,f] **Kohtaroh Miura,**[c,d,e,g] **Konstantin Ottnad,**[e,f] **Andreas Risch,**[h] **Jonas Wilhelm and Hartmut Wittig**[a,c,d,e,f]

[a] *Department of Theoretical Physics, CERN 1211 Geneva 23, Switzerland*

[b] *Aix Marseille Université, Université de Toulon, CNRS, CPT, Marseille, France*

[c] *Helmholtz-Institut Mainz, Johannes Gutenberg-Universität Mainz, Staudingerweg 18, 55128 Mainz, Germany*

[d] *GSI Helmholtzzentrum für Schwerionenforschung, Planckstraße 1, 64291 Darmstadt, Germany*

[e] *PRISMA$^+$ Cluster of Excellence, Johannes Gutenberg-Universität Mainz, Staudingerweg 9, 55128 Mainz, Germany*

[f] *Institut für Kernphysik, Johannes Gutenberg-Universität Mainz, Johann-Joachim-Becher-Weg 45, D 55128 Mainz, Germany*

[g] *Kobayashi-Maskawa Institute for the origin of particles and the Universe, Nagoya University Furo-cho, Chikusa-ku, Nagoya Aichi 464-8602, JAPAN*

[h] *John von Neumann-Institut für Computing NIC, Deutsches Elektronen-Synchrotron DESY, Platanenallee 6, 15738 Zeuthen, Germany*

E-mail: msanjosp@uni-mainz.de

As present and future experiments, on both the energy and precision frontiers, look to identify new physics beyond the Standard Model (BSM), we require more precise determinations of fundamental quantities, like the QED and electroweak couplings at various momenta. These can be obtained either entirely from experimental measurements, or from one such measurement at a particular virtuality combined with the couplings' virtuality dependence computed within the SM. Thus, a precise, entirely theoretical determination of the running couplings is highly desirable, even more since the preliminary results of the E989 experiment in Fermilab were published. We give results for the hadronic contribution to the QED running coupling $\alpha(Q^2)$ and weak mixing angle $\sin^2\theta_W(Q^2)$ in the space-like energy region $(0, 7]$ GeV^2 with a total relative uncertainty of 2% at energies $Q^2 \ll 1\,\text{GeV}^2$, and 1% at $Q^2 > 1\,\text{GeV}^2$.

CERN-TH-2021-126
DESY-21-137
MITP/21-038

The 38th International Symposium on Lattice Field Theory, LATTICE2021 26th-30th July, 2021 Zoom/Gather@Massachusetts Institute of Technology

*Speaker

1. Introduction

The QED running coupling at the Z-pole mass $\alpha(M_Z^2)$ enters in the electroweak global fit. It is also closely related to the leading hadronic contribution to the anomalous magnetic moment of the muon, $a_\mu^{\rm HLO}$, and both quantities can be obtained using the optical theorem and the R-ratio data, which is the cross-section $\sigma\,(e^+e^- \to \text{hadrons})$ normalized by $\sigma\,(e^+e^- \to \mu^+\mu^-)$. For an up-to-date R-ratio data collection, see [1–3]. In the near future, the MUonE experiment [4] at CERN will compute $a_\mu^{\rm HLO}$ from the running coupling via a dispersion relation.

The weak mixing angle $\sin^2\theta_W$ is a probe for BSM physics, in particular at energies much smaller than the electroweak scale $q^2 \ll M_Z^2$. It can be measured in neutrino-nucleus scattering, atomic parity violation and parity-violating lepton scattering. However, unlike α, it is known with a poor precision in this energy range. The upcoming experiments P2 at MESA [5], as well as MOLLER [6] and SoLID [7, 8] at JLab, aim to improve its precision. Hadronic effects dominate the uncertainty of both quantities, $\alpha(q^2)$ and $\sin^2\theta_W(q^2)$. In this project, we compute these contributions using a similar approach to the one employed to obtain $a_\mu^{\rm HLO}$ [9].

1.1 Main definitions

The QED coupling $\alpha(q^2)$ is parameterized in the *on-shell* scheme as

$$\alpha(q^2) = \frac{\alpha}{1 - \Delta\alpha(q^2)}, \tag{1}$$

where the fine-structure constant is denoted by α. The hadronic contribution to $\Delta\alpha(q^2)$ can be expressed in terms of a subtracted vacuum polarization function (sVPF),

$$(\Delta\alpha)_{\rm had}(q^2) = 4\pi\alpha\hat{\Pi}^{\gamma\gamma}(q^2). \tag{2}$$

In a similar fashion, to leading-order, the $\sin^2\theta_W$ can be given in the on-shell scheme as [10, 11]

$$\sin^2\theta_W(q^2) = \sin^2\theta_W\left(1 + \Delta\sin^2\theta_W(q^2)\right), \tag{3}$$

where $\sin^2\theta_W$ is evaluated at $q^2 \to 0$ and the hadronic contribution to the running is

$$(\Delta\sin^2\theta_W)_{\rm had}(q^2) = -\frac{4\pi\alpha}{\sin^2\theta_W}\hat{\Pi}^{Z\gamma}(q^2). \tag{4}$$

1.2 Time-momentum representation

Both $\hat{\Pi}^{\gamma\gamma}$ and $\hat{\Pi}^{Z\gamma}$ have an integral representation in the space-like region $Q^2 = -q^2$, which is known as the time-momentum representation (TMR) [12, 13],

$$\hat{\Pi}(Q^2) = \int_0^\infty dx_0 G(x_0) K(x_0, Q^2), \quad \text{with} \quad K(x_0, Q^2) = x_0^2 - \frac{4}{Q^2}\sin^2\left(\frac{Qx_0}{2}\right). \tag{5}$$

The kernel may be evaluated at any Q^2, but the lattice spacing and its extent limit the range of virtualities that we can reliably handle. The kernel weights the correlator depending on the virtuality input, and virtualities $Q^2 \sim (\pi/a)^2$ probe the short distances of the TMR correlator $G(x_0)$, yielding strong cut-off effects, while virtualities $Q^2 \ll 1\,\text{GeV}^2$ emphasize the long-distance part of the

correlator. We compute the two-point functions $G^{\gamma\gamma}(x_0)$ and $G^{Z\gamma}(x_0)$, which we decompose using the isospin basis plus the charm-quark component neglecting charm disconnected contributions,

$$G^{\gamma\gamma}(x_0) = G^{33}(x_0) + \frac{1}{3}G^{88}(x_0) + \frac{4}{9}C^{c,c}(x_0), \tag{6}$$

$$G^{Z\gamma}(x_0) = \left(\frac{1}{2} - \sin^2\theta_W\right) G^{\gamma\gamma}(x_0) - \frac{1}{6\sqrt{3}}G^{08}(x_0) - \frac{1}{18}C^{c,c}(x_0). \tag{7}$$

The isovector $G^{33}(x_0)$, isoscalar $G^{88}(x_0)$ and $G^{08}(x_0)$ parts can be further decomposed into individual flavour components that are directly accessible on the lattice,

$$\begin{aligned} G^{33}(x_0) &= \frac{1}{2}C^{\ell,\ell}(x_0), \\ G^{88}(x_0) &= \frac{1}{6}\left(C^{\ell,\ell}(x_0) + 2C^{s,s}(x_0) + 2D^{\ell-s,\ell-s}(x_0)\right), \\ G^{08}(x_0) &= \frac{1}{2\sqrt{3}}\left(C^{\ell,\ell}(x_0) - C^{s,s}(x_0) + D^{2\ell+s,\ell-s}(x_0)\right). \end{aligned} \tag{8}$$

$C^{\ell,\ell}$, $C^{s,s}$ and $C^{c,c}$ are the light, strange and charm quark-connected contributions, respectively. $D^{\ell-s,\ell-s}$ and $D^{2\ell+s,\ell-s}$ are the quark-disconnected pieces, which cancel at the SU(3)-flavour-symmetric point.

2. Lattice setup

We employ an extensive set of Coordinated Lattice Simulations ensembles with $N_f = 2+1$ flavours, non-perturbatively $O(a)$-improved Wilson fermions and tree-level Lüscher-Weisz gauge action [14, 15]. For the vector currents, we employ two different discretizations in order to further constrain the continuum extrapolation, the *local* (*l*) and *point-split* (*ps*), whose renormalization and improvement is explained in [16] —the latter is a conserved current, and its renormalization is trivial. Table 1 lists the ensembles used in this work. We employ four different lattice spacings and the meson masses range from $M_\pi = M_K \approx 415\,\text{MeV}$ at the SU(3)-flavour-symmetric point to the physical point, along a trajectory where the sum of the bare u, d and s quark masses is constant. The quark loops for the quark-disconnected contribution constitute the most expensive part of the computation. We compute them via a variant of the method proposed in [17] combining the one-end trick [18] with a combination of the generalized hopping parameter expansion [19] and hierarchical probing [20]. The scale is set using $\sqrt{8t_0^{\text{phy}}} = 0.415(4)(2)$ fm [15].

2.1 Analysis

We improve the signal-to-noise ratio by applying the bounding method [21] to our correlators. We employ the effective mass $M_{\text{eff}}(x_0) = \log\left(G(x_0)/G(x_0+1)\right)$ and the ground-state energy E_0,

$$0 \le G(x_0^{\text{cut}})e^{-M_{\text{eff}}(x_0)\left(x_0 - x_0^{\text{cut}}\right)} \le G(x_0) \le G(x_0^{\text{cut}})e^{-E_0\left(x_0 - x_0^{\text{cut}}\right)}, \quad x_0 \ge x_0^{\text{cut}}. \tag{9}$$

The ground state is either the ρ meson mass or the two-pion state energy for the isovector contribution. For the isoscalar component, it is either the three-pion state or the ω meson mass. We estimate the former via its non-interacting energy [22] and the latter employing $M_\rho \approx M_\omega$. We find M_ρ is

	T/a	L/a	$t_0^{\rm sym}/a^2$	a [fm]	L [fm]	M_π, M_K [MeV]	$M_\pi L$	# cnfg (con., dis., charm)
H101	96	32	2.86	0.08636	2.8	418	5.9	2000 - 1000
H102	96	32			2.8	353 438	4.9	1900 1900 975
H105*	96	32			2.8	281 463	3.9	1000 1000 500
N101	128	48			4.1	279 461	5.9	1155 1155 345
C101	96	48			4.1	219 470	4.6	2000 2000 400
B450	64	32	3.659	0.07634	2.4	414	5.1	1600 - 800
S400	128	32			2.4	351 441	4.3	1720 1720 800
N451	128	48			3.7	286 460	5.3	1000 1000 200
D450	128	64			4.9	216 475	5.3	500 500 300
H200*	96	32	5.164	0.06426	2.1	418	4.4	1980 - 480
N202	128	48			3.1	411	6.4	875 - 420
N203	128	48			3.1	345 442	5.4	1500 1500 700
N200	128	48			3.1	283 462	4.4	1695 1695 390
D200	128	64			4.1	201 480	4.2	2000 1000 500
E250	192	96			6.2	129 489	4.1	485 485 65
N300	128	48	8.595	0.04981	2.4	422	5.1	1680 - 480
N302	128	48			2.4	346 451	4.2	2190 1080 480
J303	192	64			3.2	257 474	4.2	1040 1040 100
E300	192	96			4.8	175 491	4.2	600 300 100

Table 1: Set of Coordinated Lattice Simulations (CLS) ensembles used in this work. For each one, we give name, geometry, scale in different units, physical size, meson masses and statistics used, differentiating between the connected light and strange contributions, the disconnected pieces and the charm component. We also give $M_\pi L$, as it is related to the size of the finite-size effects present. Ensembles H105 and H200 are only used in the study of the latter, and do not enter the final analysis.

always lighter and use it as the upper bound. Figure 1 shows the result of the bounding procedure at the physical pion mass and energy $Q^2 = 0.5\,\text{GeV}^2$. On the LHS, we show the isovector component and, on the RHS, the isoscalar. The two sets of points indicate the upper and lower bound, while the two vertical lines show the averaged interval and the cyan band is the improved estimate for $\hat{\Pi}$.

To estimate the finite-size corrections we employed two different methods, the Hansen-Patella (HP) procedure [23, 24] and the Meyer-Lellouch-Lüscher (MLL) method [25–27], using for the latter the Gounaris-Sakurai (GS) parameterization of the vector pion form factor $F_\pi(\omega^2)$ [28]. MLL estimates the amplitudes and energies of the finite-size correlator below the inelastic threshold,

$$G(x_0, L) = \sum_n |A_n|^2 e^{-\omega_n x_0}, \tag{10}$$

where $|A_n|^2$ is related to the module of $F_\pi(\omega^2)$, and ω_n to its phase via the Lüscher equation. The infinite-volume correlator can be expressed via the continuous spectral representation

$$G(x_0) = \int_0^\infty d\omega \omega^2 \rho(\omega^2) e^{-\omega|x_0|}, \quad \rho(\omega^2) = \frac{1}{48\pi^2}\left(1 - \frac{4M_\pi^2}{\omega^2}\right)^{3/2} \left|F_\pi(\omega^2)\right|^2 \quad x_0 \neq 0. \tag{11}$$

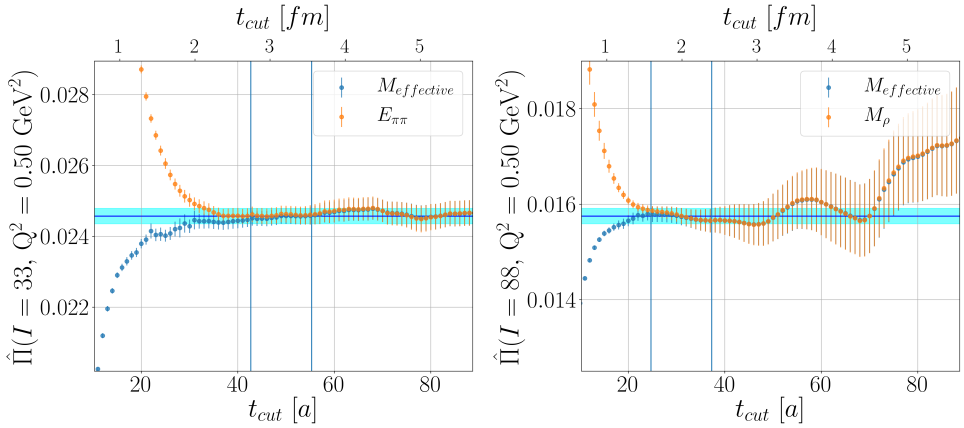

Figure 1: Bounding method applied at the physical pion mass (ensemble E250) and $Q^2 = 0.5\,\mathrm{GeV}^2$. The data-points indicate the bounds as a function of t_{cut}, the interval where both are averaged is given between the vertical lines, and the improved estimate is given by the cyan band. LHS: isovector component. RHS: isoscalar contribution.

Finally, we take $G(x_0) - G(x_0, L)$ as the finite-size correction for each time-slice x_0. We split the correlator in the time slice $x_i = (M_\pi L/4)^2 / M_\pi$, which estimates when the spectral representation of the correlator starts to be described by a handful of states. We employ the HP method for $x_0 < x_i$, and for $x_0 \geq x_i$ both HP and MLL give compatible results. For two of our ensembles that have the same parameters but the size, H105 and N101, we find a finite-size correction of $\sim 2\%$ for the first, and of $\sim 0.2\%$ for the second, at $Q^2 = 1\,\mathrm{GeV}^2$.

We perform an extrapolation to the physical point $a \to 0$, $M_\pi^{\mathrm{phy}} = 134.9768(5)\,\mathrm{MeV}$, $M_K^{\mathrm{phy}} = 495.011(15)\,\mathrm{MeV}$, where we employ the meson masses without isospin breaking (IB) effects [29, 30], since they are absent in our calculation. We employ the dimensionless variables [15] $a^2/8t_0^{\mathrm{sym}}$, $\phi_2 = 8t_0 M_\pi^2$, and $\phi_4 = 8t_0\left(M_\pi^2/2 + M_K^2\right)$. We extrapolate the isovector and isoscalar components together, as they coincide in the SU(3)-flavour-symmetric point, where in fact $\phi_4^{\mathrm{sym}} = 3\phi_2^{\mathrm{sym}}/2$. The fit model of each isospin and correlator discretization can be divided into lattice- and mass-dependent terms, $\hat{\Pi}(a, \phi_2, \phi_4; d, i) = \hat{\Pi}_{\mathrm{continuum}}(a; d) + \hat{\Pi}_{\mathrm{mass}}(\phi_2, \phi_4; i)$,

$$\hat{\Pi}_{\mathrm{continuum}}(a; d) = \begin{cases} \hat{\Pi}^{\mathrm{sym}} + \alpha_{2,d}\left(a^2/8t_0^{\mathrm{sym}}\right), & Q^2 \lesssim 2.5\,\mathrm{GeV}^2, \\ \hat{\Pi}^{\mathrm{sym}} + \alpha_{2,d}\left(a^2/8t_0^{\mathrm{sym}}\right) + \alpha_{3,d}\left(a^2/8t_0^{\mathrm{sym}}\right)^{3/2}, & Q^2 \gtrsim 2.5\,\mathrm{GeV}^2, \end{cases} \tag{12}$$

$$\hat{\Pi}_{\mathrm{mass}}(\phi_2, \phi_4; i) = \beta_{1,i}\left(\phi_2 - \phi_2^{\mathrm{sym}}\right) + \delta\left(\phi_4 - 3\phi_2^{\mathrm{sym}}/2\right) + \begin{cases} \beta_{2,33}\log\left(\phi_2/\phi_2^{\mathrm{sym}}\right), & i = 33, \\ \beta_{2,88}\left(\phi_2 - \phi_2^{\mathrm{sym}}\right)^2, & i = 88. \end{cases} \tag{13}$$

The subscript $d = ps, l$ runs over the correlator discretizations and $i = 33, 88$ over both isospins. Therefore, there is one pair of α_2 and α_3 parameters per correlator discretization, and one set of parameters β_1 and β_2 per isospin. Also, the curvature of the data is described differently for the isovector and isoscalar components. Figure 2 shows the extrapolation to the physical point for the isovector, isoscalar and charm components at $Q^2 = 1\,\mathrm{GeV}^2$. The different colours indicate the various lattice spacings, the dashed and dotted lines refer to the two correlator discretizations. The

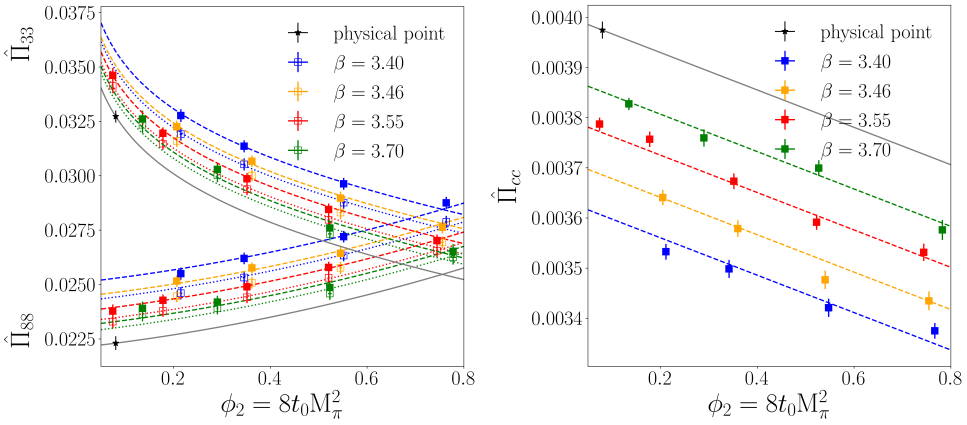

Figure 2: Extrapolation to the physical point at $Q^2 = 1\,\text{GeV}^2$. The isovector and isoscalar components are represented on the LHS and the charm contribution on the RHS.

grey line is the continuum extrapolation, with the black dot indicating the result at the physical point. For the charm contribution, the *local* discretization shows much larger artefacts, therefore we only extrapolate the *ps* data. The model employed is $\hat{\Pi}(a, \phi_2; \text{charm}) = \hat{\Pi}^{\text{phy}} + \alpha_{2,ps}\left(a^2/8t_0^{\text{sym}}\right) + \beta_{1,\text{charm}}\left(\phi_2 - \phi_2^{\text{phy}}\right)$. The 08 component is found to be rather insensitive to the lattice spacing, and thus we only study the *ps* discretization. Besides, eq. (8) anticipates this contribution to be zero at the SU(3)-flavour-symmetric point. It suffices to use the one-parameter model $\hat{\Pi}(\phi_2, \phi_4; 08) = \hat{\Pi}_{08}\,(\phi_4 - 3\phi_2/2) = \hat{\Pi}_{08} 8t_0\left(M_K^2 - M_\pi^2\right)$. To assess the extrapolation's systematic error, we exclude all ensembles with pion masses $M_\pi > 400\,\text{MeV}$, corresponding to approximately $\phi_2 > 0.6$ in fig. 2. In the case of the charm and 08 components, we also cut all masses $M_\pi > 300\,\text{MeV}$, or $\phi_2 > 0.4$. The fit quality at $Q^2 = 1\,\text{GeV}^2$ is $\chi^2/\text{ddof} = 1.35$ for the isovector and isoscalar, $\chi^2/\text{ddof} = 0.66$ for the 08 term, and $\chi^2/\text{ddof} = 2.5$ for the charm contribution. For the latter, the mass cuts significantly improve the fit quality to $\chi^2/\text{ddof} = 0.85$ without changing the result at the physical point, suggesting the bad fit quality is an artifact of the covariance matrix.

3. Results

Figure 3 shows our preliminary results for the hadronic contributions at the physical point of both, the QED running coupling and the weak mixing angle, defined in eqs. (2) and (4) respectively. Following eq. (8), we present the result of each isospin component, including e.g. the prefactors 1/3 and 4/9 of eq. (6) to emphasize the light-quark correlator's dominance. The width shows our total error budget. The QED and strong isospin breaking corrections have been computed for a small subset of ensembles [31–33]. We use them to estimate the systematic uncertainty due to the absence of IB effects in our main computation. The error size for $(\Delta\alpha)_{\text{had}}$ varies between 1% at small energies and 0.5% at the highest momentum probed while, in the case of $(\Delta\sin^2\theta_W)_{\text{had}}$, it is one order of magnitude smaller, between 0.1% and 0.05%, respectively. The scale setting error, which enters through $8t_0^{\text{phy}}Q^2$ in the kernel $K(x_0, Q^2)$ of eq. (5) and the definition of the physical point, is estimated to be $\sim 0.5\%$, using bootstrap sampling.

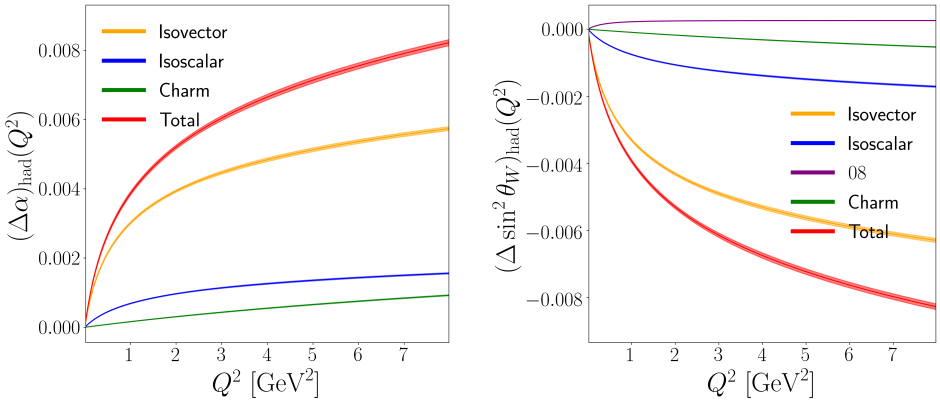

Figure 3: Results for eq. (2) (LHS) and eq. (4) (RHS) at the physical point. We differentiate between the various contributions according to eqs. (6) and (7), including all prefactors.

4. Conclusions

In this work, we compute the hadronic contribution to the QED running coupling $\alpha(Q^2)$ and weak mixing angle $\sin^2\theta_W(Q^2)$ in the space-like energy region $(0, 7]$ GeV^2. Our main error sources stem from statistics, the scale setting, the extrapolation to the physical point and the isospin breaking corrections, giving a total relative uncertainty of 2% at energies $Q^2 \ll 1\,\text{GeV}^2$, and 1% for the range $Q^2 > 1\,\text{GeV}^2$. A preliminary comparison shows rough agreement between our determination of $\alpha(Q^2)$ and the Lattice results [10, 21]. Currently, we aim to compare our QED running coupling with the phenomenological determinations [1–3], as well as our $\sin^2\theta_W$ with [2, 34]. The QED and strong isospin breaking effects have been computed on a subset of ensembles so that we may estimate the uncertainty due to their absence in the main computation, but the analysis will be extended to other ensembles in the future [32, 33, 35]. We plan to express fig. 3 in an analytic form, employing a rational expression for the running. [36] shows how our results affect $\Delta\alpha(M_Z^2)$.

References

[1] M. Davier, A. Hoecker, B. Malaescu and Z. Zhang, *A new evaluation of the hadronic vacuum polarisation contributions to the muon anomalous magnetic moment and to* $\alpha(m_Z^2)$, *Eur. Phys. J. C* **80** (2020) 241 [1908.00921].

[2] F. Jegerlehner, $\alpha_{QED,\,eff}(s)$ *for precision physics at the FCC-ee/ILC*, *CERN Yellow Reports: Monographs* **3** (2020) 9.

[3] A. Keshavarzi, D. Nomura and T. Teubner, $g-2$ *of charged leptons,* $\alpha(M_Z^2)$ *, and the hyperfine splitting of muonium*, *Phys. Rev. D* **101** (2020) 014029 [1911.00367].

[4] G. Abbiendi et al., *Measuring the leading hadronic contribution to the muon g-2 via μe scattering*, *Eur. Phys. J.* **C77** (2017) 139 [1609.08987].

[5] D. Becker et al., *The P2 experiment*, *Eur. Phys. J. A* **54** (2018) 208 [1802.04759].

[6] MOLLER collaboration, *The MOLLER Experiment: An Ultra-Precise Measurement of the Weak Mixing Angle Using Møller Scattering*, 1411.4088.

[7] SoLID collaboration, *A White Paper on SoLID (Solenoidal Large Intensity Device)*, 1409.7741.

[8] P.A. Souder, *Parity violation in deep inelastic scattering with the solid spectrometer at jlab*, *IJMP Conf. Series* **40** (2016) 1660077.

[9] A. Gérardin, M. Cè, G. von Hippel, B. Hörz, H.B. Meyer, D. Mohler et al., *The leading hadronic contribution to* $(g-2)_\mu$ *from lattice QCD with* $N_\mathrm{f} = 2+1$ *flavours of O(a) improved Wilson quarks*, *Phys. Rev. D* **100** (2019) 014510 [1904.03120].

[10] F. Burger, K. Jansen, M. Petschlies and G. Pientka, *Leading hadronic contributions to the running of the electroweak coupling constants from lattice QCD*, *JHEP* **11** (2015) 215 [1505.03283].

[11] F. Jegerlehner, *Hadronic Contributions to Electroweak Parameter Shifts: A Detailed Analysis*, *Z. Phys. C* **32** (1986) 195.

[12] A. Francis, B. Jäger, H.B. Meyer and H. Wittig, *New representation of the Adler function for lattice QCD*, *Phys. Rev. D* **88** (2013) 054502 [1306.2532].

[13] D. Bernecker and H.B. Meyer, *Vector correlators in lattice QCD: Methods and applications*, *European Physical Journal A* **47** (2011) 148 [1107.4388].

[14] M. Bruno et al., *Simulation of QCD with* $N_f = 2+1$ *flavors of non-perturbatively improved Wilson fermions*, *JHEP* **02** (2015) 043 [1411.3982].

[15] M. Bruno, T. Korzec and S. Schaefer, *Setting the scale for the CLS* $2+1$ *flavor ensembles*, *Phys. Rev. D* **95** (2017) 074504 [1608.08900].

[16] A. Gérardin, T. Harris and H.B. Meyer, *Nonperturbative renormalization and* $O(a)$*-improvement of the nonsinglet vector current with* $N_f = 2+1$ *Wilson fermions and tree-level Symanzik improved gauge action*, *Phys. Rev. D* **99** (2019) 014519 [1811.08209].

[17] L. Giusti, T. Harris, A. Nada and S. Schaefer, *Frequency-splitting estimators of single-propagator traces*, *Eur. Phys. J. C* **79** (2019) 586 [1903.10447].

[18] UKQCD collaboration, *Decay width of light quark hybrid meson from the lattice*, *Phys. Rev. D* **73** (2006) 074506 [hep-lat/0603007].

[19] V. Gülpers, G. von Hippel and H. Wittig, *Scalar pion form factor in two-flavor lattice QCD*, *Phys. Rev. D* **89** (2014) 094503 [1309.2104].

[20] A. Stathopoulos, J. Laeuchli and K. Orginos, *Hierarchical probing for estimating the trace of the matrix inverse on toroidal lattices*, 1302.4018.

[21] Budapest-Marseille-Wuppertal collaboration, *Hadronic vacuum polarization contribution to the anomalous magnetic moments of leptons from first principles*, *Phys. Rev. Lett.* **121** (2018) 022002 [1711.04980].

[22] M.T. Hansen, F. Romero-López and S.R. Sharpe, *Generalizing the relativistic quantization condition to include all three-pion isospin channels*, *JHEP* **07** (2020) 047 [2003.10974].

[23] M.T. Hansen and A. Patella, *Finite-volume effects in* $(g-2)_\mu^{HVP,LO}$, *Phys. Rev. Lett.* **123** (2019) 172001 [1904.10010].

[24] M.T. Hansen and A. Patella, *Finite-volume and thermal effects in the leading-HVP contribution to muonic* $(g-2)$, *JHEP* **10** (2020) 029 [2004.03935].

[25] H.B. Meyer, *Lattice QCD and the Timelike Pion Form Factor*, *Phys. Rev. Lett.* **107** (2011) 072002 [1105.1892].

[26] L. Lellouch and M. Lüscher, *Weak transition matrix elements from finite volume correlation functions*, *Commun. Math. Phys.* **219** (2001) 31 [hep-lat/0003023].

[27] M. Lüscher, *Signatures of unstable particles in finite volume*, *Nucl. Phys. B* **364** (1991) 237.

[28] G.J. Gounaris and J.J. Sakurai, *Finite-width corrections to the vector-meson-dominance prediction for* $\rho \to e^+e^-$, *Phys. Rev. Lett.* **21** (1968) 244.

[29] T. Blum, G. Colangelo, A. El Khadra, C. Lehner, L. Lellouch, H. Meyer et al., "Discussion: Criteria for inclusion in WP update, Muon $g-2$ Theory Initiative workshop, 30/06/2021 at 15:05 CEST."

[30] Particle Data Group collaboration, *Review of Particle Physics*, *PTEP* **2020** (2020) 083C01.

[31] A. Risch and H. Wittig, *Towards leading isospin breaking effects in mesonic masses with* $O(a)$ *improved Wilson fermions*, *EPJ Web Conf.* **175** (2018) 14019 [1710.06801].

[32] A. Risch and H. Wittig, *Towards leading isospin breaking effects in mesonic masses with open boundaries*, *PoS* **LATTICE2018** (2018) 059 [1811.00895].

[33] A. Risch and H. Wittig, *Leading isospin breaking effects in the hadronic vacuum polarisation with open boundaries*, *PoS* **LATTICE2019** (2019) 296 [1911.04230].

[34] F. Jegerlehner, *Electroweak effective couplings for future precision experiments*, *Nuovo Cim. C* **034S1** (2011) 31 [1107.4683].

[35] A. Risch and H. Wittig, *Leading isospin breaking effects in the HVP contribution to* a_μ *and the running of* α, *PoS* **LATTICE2021** (2021) 106.

[36] K. Miura, M. Cè, A. Gérardin, H. Meyer, A. Risch, M. San José Pérez et al., "HVP contribution to running coupling and electroweak precision science." https://indi.to/ZTQst, 2021.